Journal of Biosciences and Medicines, 2026, 14(9), 364-380
https://www.scirp.org/journal/jbm
ISSN Online: 2327-509X
ISSN Print: 2327-5081

Computational Fluid Dynamics for Assessing Intracranial Aneurysm Formation, Progression, and Rupture

Zixuan Deng, Ruolin Xiao, Jing Luo, Xiujuan Liu*

Department of Radiology, Zhuhai Clinical Medical College of Jinan University (Zhuhai People's Hospital, The Affiliated Hospital of Beijing Institute of Technology), Zhuhai, China
Email: *liuxiujuan2005@126.com

How to cite this paper: Deng, Z.X., Xiao, R.L., Luo, J. and Liu, X.J. (2026) Computational Fluid Dynamics for Assessing Intracranial Aneurysm Formation, Progression, and Rupture. *Journal of Biosciences and Medicines*, **14**, 364-380.
https://doi.org/10.4236/jbm.2026.149022

Received: August 3, 2026
Accepted: September 14, 2026
Published: September 17, 2026

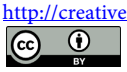

Abstract

Intracranial aneurysms (IAs) are often likened to "time bombs" within the human brain, as they may rupture unpredictably once entering an unstable state. Elucidation of the mechanisms underlying IA formation and progression is essential for understanding aneurysm instability. The formation and evolution of IAs have been shown to be closely associated with hemodynamic factors. Computational fluid dynamics (CFD), by enabling the simulation of patient-specific hemodynamic environments, has identified a range of qualitative and quantitative hemodynamic parameters that play critical roles in the formation, progression, and rupture of IAs. These advances provide important insights into the assessment of rupture risk. In the future, CFD is expected to be integrated with emerging medical imaging techniques and artificial intelligence in a multimodal framework, combined with longitudinal follow-up data, to establish more robust and accurate tools for IA rupture risk prediction.

Keywords

Intracranial Aneurysm, Computational Fluid Dynamics, Hemodynamics, Aneurysm Growth, Rupture Risk

1. Introduction

Intracranial aneurysm (IA) is defined as a localized, abnormal dilation of the intracranial arterial wall, forming a sac-like protrusion. As a common and life-threatening cerebrovascular disorder, its incidence ranks second only to cerebral thrombosis and hypertensive intracerebral hemorrhage among cerebrovascular events [1]. Rupture of an IA can result in spontaneous subarachnoid hemorrhage

(SAH), which is associated with high rates of disability and mortality: the combined mortality and disability rate is approximately 30% after the initial rupture and increases to nearly 70% following rebleeding [2]. Currently, ruptured IAs are primarily managed by surgical clipping or endovascular intervention. However, the identification of high-risk unruptured IAs and the optimal timing of intervention remain significant clinical challenges.

At present, commonly used clinical scoring systems, including PHASES and ELAPSS, are applied to assess rupture risk in unruptured IAs. These scoring systems are summarized in Table 1.

Table 1. Clinical risk scoring systems for rupture assessment of unruptured intracranial aneurysms.

Juvela (2019 Stroke)			PHASES (2014 Lancet)			ELAPSS (2017 Neurology)		
Risk factors for rupture	Group	Points	Risk factors for rupture	Group	Points	Aneurysm growth risk score	Group	Points
Age	<40 years	2	Age	<70 years	0	Age	≤60 years	0
	≥40 years	0		≥70 years	1		>60 years	1
Size of aneurysm (mm)	≥7.0	3	Size of aneurysm (mm)	<7.0	0	Size of aneurysm (mm)	1.0 - 2.9	0
	<7.0	0		7.0 - 9.9	3		3.0 - 4.9	4
				10.0 - 19.9	6		5.0 - 6.9	10
				≥20.0	10		7.0 - 9.9	13
							≥10.0	22
Site of the aneurysm	ACom	5	Site of the aneurysm	ICA	0	Site of the aneurysm	ICA/ACA/Acom	0
	ICA bifurcation	4		MCA	2		MCA	3
	PCom	2		ACA/Pcom/posterior	4		Pcom/posterior	5
	Others	0						
Cigarette smoking at baseline	Yes	2	Population	North American, European (other than Finnish)	0	Population	North American, Chinese, European (other than Finnish)	0
	No	0		Japanese	3		Japanese	1
				Finnish	5		Finnish	7
			Earlier SAH from another aneurysm	No	0	Earlier SAH	Yes	0
				Yes	1		No	1
			Hypertension	No	0	Shape of aneurysm	Regular	0
				Yes	1		Irregular	4

These approaches largely rely on limited morphological features and clinical variables, resulting in a narrow assessment scope, insufficient representation of inter-individual variability, and a lack of dynamic temporal resolution, thereby limiting their ability to achieve precise, individualized risk stratification.

In fact, the hemodynamic environment plays a critical role in the initiation and progression of IAs [3]. The predilection of IAs for arterial bifurcations within the Circle of Willis further supports this hemodynamic hypothesis. However, conventional imaging techniques are limited to visualizing static anatomical structures and are incapable of capturing hemodynamic characteristics. In recent years, computational fluid dynamics (CFD) simulation has increasingly emerged as an important tool for evaluating the hemodynamic features of IAs [4]. Based on medical imaging data, CFD enables the simulation of blood flow dynamics and the quantification of hemodynamic parameters, thereby facilitating a comprehensive assessment of the aneurysmal hemodynamic environment.

To provide an overview of the current state of research, this review synthesizes recent domestic and international studies to summarize the advances in CFD-based investigations of IA formation and progression.

2. Overview of CFD and Related Parameters

2.1. Overview of CFD and Its Development

Hemodynamics, as an important branch of biomechanics, focuses on the patterns and regulatory mechanisms of blood flow within the cardiovascular and cerebrovascular systems. CFD has been widely adopted as a principal approach for characterizing hemodynamic behavior [5]. By employing numerical methods and computer-based algorithms to solve governing fluid equations, such as the Navier-Stokes equations, CFD enables the simulation and analysis of complex flow phenomena.

This approach is typically based on medical imaging data acquired from modalities such as computed tomography angiography (CTA) and magnetic resonance angiography (MRA). The acquired images are processed using three-dimensional reconstruction software, such as Mimics and 3D Slicer, to perform segmentation and reconstruction, thereby generating patient-specific geometric models of the aneurysm and the parent vessel. Following model reconstruction, mesh generation is performed to create computational grids suitable for CFD analysis. Boundary conditions are then prescribed, allowing for the analysis of complex flow structures and extraction of detailed hemodynamic parameters within the aneurysm.

CFD simulations require the specification of boundary conditions, fluid models, and simulation types, which are determined by the clinical objectives, desired parameter accuracy, and available computational resources and time constraints. Boundary conditions typically include inlet and outlet flow parameters as well as vessel wall properties. Fluid models are generally categorized as Newtonian or non-Newtonian. The Newtonian model assumes constant viscosity and is com-

monly used in vascular studies due to its computational simplicity, whereas the non-Newtonian model accounts for variable viscosity and more accurately reflects hemodynamic characteristics in low shear regions, thereby potentially improving the accuracy of rupture risk assessment. However, its higher computational cost and dependence on specialized software have limited its widespread clinical application. With respect to temporal resolution, simulations may be conducted under steady-state or transient conditions. Steady-state simulations assume constant inflow conditions that do not vary over the cardiac cycle, whereas transient simulations incorporate physiologically realistic pulsatile flow waveforms, enabling the capture of time-dependent hemodynamic parameters associated with the cardiac cycle [6].

Nevertheless, CFD simulations remain subject to methodological uncertainties arising from model reconstruction procedures and simulation assumptions. Variations in image segmentation approaches may lead to differences in reconstructed aneurysm geometry, while discrepancies in mesh resolution may affect the accuracy of calculated hemodynamic parameters. In addition, differences among studies in the specification of inlet and outlet boundary conditions, blood rheological models, and vessel wall assumptions may contribute to variability in CFD-derived hemodynamic parameters. Furthermore, the lack of patient-specific input data in many studies may further reduce simulation precision and introduce discrepancies between simulated and actual hemodynamic conditions [7]. Therefore, these methodological factors should be carefully considered when interpreting the findings of CFD studies.

In recent years, four-dimensional flow magnetic resonance imaging (4D Flow MRI) has emerged as an advanced imaging modality capable of providing real-time qualitative and quantitative assessment of hemodynamics based on in vivo measurements [8]. The integration of CFD simulations with 4D Flow MRI data is expected to enhance physiological fidelity and improve the accuracy of derived parameters. Given the relatively limited spatial resolution of 4D Flow MRI, the development of super-resolution reconstruction algorithms that integrate artificial intelligence with CFD techniques has become an important area of research. Furthermore, transcranial Doppler ultrasound (TCD) can provide patient-specific inflow boundary conditions for CFD models of IAs. The combined application of these techniques may help mitigate simulation inaccuracies and address the lack of individualized data in conventional CFD modeling [9].

2.2. Overview of CFD-Related Parameters

When CFD is applied to the study of IAs, hemodynamic characteristics can be revealed from diverse dimensions via qualitative and quantitative analysis.

Qualitative analysis serves as a fundamental component of hemodynamic assessment. Blood flow trajectories are simulated through numerical computation and visualized in the form of streamlines, enabling an intuitive representation of intra-aneurysmal flow patterns. Key qualitative features include flow stability,

complexity, concentration, and the spatial extent of impingement regions. Accordingly, qualitative descriptors such as inflow jets, vortex structures, and flow impingement zones can be identified. Representative qualitative parameters are illustrated in Figure 1 [10].

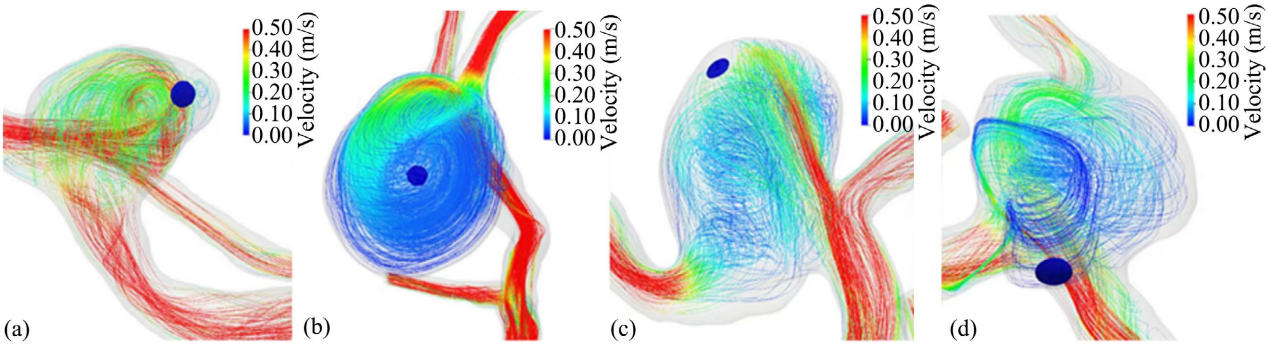

Figure 1. Schematic representation of qualitative hemodynamic parameters in four ruptured intracranial aneurysms. Blue circles indicate rupture sites. (a) The inflow jet does not directly impinge on the aneurysm wall; the rupture site is located adjacent to a vortex. (b) Overall intra-aneurysmal flow velocity is low; the vortex is located in the mid-region of the aneurysm sac. (c) Streamlines demonstrate a direct inflow jet into the aneurysm sac; the rupture site is located within the flow impingement region adjacent to the inflow jet. (d) The bleb region exhibits low flow velocity without obvious vortex formation or inflow jet.

Quantitative analysis is performed on the basis of qualitative assessment, in which hemodynamic characteristics are expressed in precise numerical terms. Following the reconstruction of three-dimensional aneurysm geometries and completion of flow field simulations, post-processing techniques are applied to calculate multiple hemodynamic parameters. These parameters convert the descriptive findings of qualitative analysis into objective numerical data, enabling accurate quantification of variables such as wall shear stress magnitude and flow concentration. Commonly used quantitative hemodynamic parameters are summarized in Table 2.

Table 2. Common quantitative hemodynamic parameters used in CFD studies of intracranial aneurysms and their definitions.

Parameters	Definition
Wall Shear Stress and Basic Derived Parameters	
Wall shear stress (WSS) [11]	Tangential frictional force exerted by blood flow on the aneurysm or arterial wall.
Time-averaged wall shear stress (TAWSS) [12]	Time-averaged magnitude of the WSS vector over a complete cardiac cycle.
Maximum wall shear stress (MWSS) [13]	Maximum WSS value within the aneurysm region.
Peak wall shear stress (PWSS) [10]	Peak WSS value observed during a single cardiac cycle.
Peak wall shear stress (WSSD) [11]	Indicator of local tensile and compressive stresses acting on the arterial wall.
Transverse wall shear stress (transWSS) [14] [15]	Quantifies multidirectional disturbances in WSS perpendicular to the primary flow direction.

Continued

Normalized WSS and Spatial Variation Parameters	
Normalized wall shear stress (NWSS) [11]	Ratio of local aneurysmal WSS to WSS in the parent artery.
Normalized wall shear stress divergence (NWSSD) [11]	Dimensionless form of WSSD normalized to parent vessel conditions.
Wall shear stress gradient (WSSG) [16]	Spatial gradient of WSS magnitude along the flow direction.
Time-averaged wall shear stress gradient (TAWSSG) [16]	Time-averaged WSSG over the cardiac cycle, typically evaluated in the aneurysm dome.
Normalized transverse wall shear stress (NtransWSS) [15]	Dimensionless ratio of transWSS to TAWSS.
Shear Oscillation and Directional Change Parameters	
Oscillatory shear index (OSI) [11]	Quantifies directional changes of WSS over the cardiac cycle.
Gradient Oscillatory Number (GON) [17]	Measures oscillatory tensile and compressive forces acting on endothelial cells.
Endothelial cell activation potential (ECAP) [12]	Ratio of OSI to TAWSS, reflecting the propensity for endothelial dysfunction and thrombosis.
Parameters of low/high shear region and area distribution	
Low shear-stress area (LSA) [10] [13]	Proportion of aneurysm surface exposed to abnormally low WSS; commonly defined as area with WSS below one standard deviation of the parent artery mean WSS [13], or area with WSS < 10% of the spatially averaged WSS within the aneurysm [10].
Low shear area ratio (LSAR) [16]	Ratio of aneurysm wall area exposed to WSS < 10% of the mean parent artery WSS.
Low shear index (LSI) [11]	Relative contribution of abnormally low WSS regions to the total shear force.
Mean-thresholded low shear area (MTLSAx%) [18]	Dimensionless area of the aneurysm where TAWSS is below x% of the mean TAWSS in the parent artery.
High shear concentration ratio (HSCR) [19]	$\mathrm{HSCR} = \left(\tau_h/\tau_D\right)/\left(A_h/A_D\right)$, where τ_h is the value of time averaged WSS in the high shear area (HSA), τ_D is the value of time averaged WSS in the entire dome, A_h is the area of the HSA, and A_D is the area of the entire dome.
Shear concentration index (SCI) [13]	Degree of spatial concentration of WSS; high-WSS regions are defined as areas where WSS exceeds the mean WSS of the adjacent parent vessel by one standard deviation.
Blood Flow Residence and Inflow Parameters	
Relative residence time (RRT) [16]	Quantifies the residence time of blood flow within the aneurysm, reflecting flow stagnation and disturbance.
Inflow concentration index (ICI) [13]	Measures the degree of concentration of the inflow jet entering the aneurysm sac.
Volume flow rat (VFR) [11]	Ratio of volumetric flow entering the aneurysm to that in the parent artery.

Continued

Pressure- and Energy-Related Parameters	
Pressure difference (PD) [20]	Normalized pressure elevation at the aneurysm wall, calculated as the difference between maximum and mean pressure divided by inlet dynamic pressure.
Pressure loss coefficient (PLc) [11]	Quantifies pressure loss across the aneurysm-bearing arterial segment.
Viscous dissipation ratio (VDR) [13]	Ratio of energy dissipated by viscous effects within the aneurysm to that in the adjacent parent artery.
Kinetic energy ratio (KER) [13]	Ratio of kinetic energy within the aneurysm to that in the adjacent parent artery.
Energy loss (EL) [11]	Total energy loss across the aneurysm-containing arterial segment.

Through the combined application of qualitative analysis, which characterizes intra-aneurysmal flow patterns, and quantitative analysis, which enables precise measurement of key hemodynamic variables, CFD provides comprehensive support for the investigation of IA hemodynamics and rupture risk assessment.

3. Research Progress on CFD-Based Assessment of Intracranial Aneurysm Formation

In the investigation of IA formation, the role of hemodynamic factors has been recognized as essential. It is well established that IAs preferentially develop at arterial bifurcations or at the apex of arterial curvatures, where vessels are exposed to concentrated hemodynamic impingement. However, research on IA initiation remains relatively limited, largely because the formation process is often difficult to identify and evaluate in vivo, posing significant challenges for early diagnosis.

Initially, hemodynamic studies of IA formation were primarily based on animal experiments. In the late 20th century, particle-tracking techniques applied in rat models demonstrated that marked particle residence and reduced flow velocity were present at sites of early aneurysm formation, with WSS observed to be highest at the distal region of the aneurysm [21]. In 2007, Meng *et al.* [22] established a canine carotid bifurcation model and, in combination with CFD analysis, demonstrated that IAs tended to develop in regions near the bifurcation apex where high WSS coexisted with high WSSG. It was suggested that the synergistic effect of elevated WSS and WSSG contributed to early aneurysm initiation. A higher WSSG indicates more pronounced spatial variation in flow, which may impose excessive biomechanical stress on localized vessel wall regions, thereby facilitating aneurysm formation. These experimental findings suggested that elevated WSS may serve as a potential biomechanical biomarker for IA initiation.

Clinical studies have further supported these observations. In 2016, Can *et al.* [23] conducted a systematic review and meta-analysis and reported that elevated WSS and high GON were closely associated with aneurysm formation at arterial bifurcations. In 2022, a case study involving longitudinal imaging follow-up of two patients demonstrated that, prior to aneurysm formation, localized blood

flow exhibited concentrated high-velocity inflow and prominent vortex structures. In these regions, WSS and WSSG were significantly higher than those in the parent artery, further supporting the critical role of elevated WSS in IA initiation [24].

More recently, in 2024, Yang *et al.* [25] combined CFD with fluid-structure interaction (FSI) analysis in a cohort of 58 unilateral internal carotid artery aneurysms. It was demonstrated that aneurysms tended to form in regions characterized by the coexistence of high WSS and high mechanical strain. In contrast, in the contralateral non-aneurysmal arteries, regions with elevated WSS usually lacked high mechanical strain, suggesting that elevated WSS alone may be insufficient to trigger aneurysm formation.

4. Research Progress on CFD-Based Assessment of Intracranial Aneurysm Growth

Aneurysm growth is recognized as one of the key risk factors for IA rupture [26]. IA growth is generally defined as the occurrence of one or more morphological changes during follow-up, including an increase in maximum diameter, the development of new blebs, or progressive morphological irregularity. In most studies, growth has been operationally defined as an increase in aneurysm maximum diameter of 0.5 mm or 1 mm on serial imaging follow-up [15] [18] [19] [27]-[30]. It has been proposed that IA growth is determined by the interaction among local hemodynamic forces, biomechanical conditions, and pathophysiological processes, with abnormal hemodynamic alterations—particularly WSS—playing a dominant role [31]. Accordingly, multiple hemodynamic parameters derived from WSS have also been used to characterize intra-aneurysmal flow conditions.

In 2017, Brinjikji *et al.* [27] analyzed 12 pairs of size- and location-matched unruptured IAs and found that the LSA in unstable aneurysms (those demonstrating growth or rupture) was 2.26 times larger than that in stable aneurysms, suggesting that an expanded low-shear region may reflect aneurysm instability. In 2022, Cornelissen *et al.* [28] expanded the sample size and conducted follow-up analysis of 31 growing aneurysms. A decrease in NWSS and increases in OSI and LSA were observed after aneurysm growth. It was hypothesized that low WSS may promote aneurysm progression by inducing local vascular inflammation, degenerative wall remodeling, and wall thinning. In 2023, Weiss *et al.* [18] studied 11 growing aneurysms and 11 size- and location-matched stable aneurysms and found that the MTLSA 70% at the aneurysm dome was significantly higher in growing aneurysms, further suggesting that expansion of low-shear regions is associated with aneurysm growth.

However, contradictory evidence has also been reported, indicating that high WSS may be associated with aneurysm growth. In 2018, Wang *et al.* [32] reported a longitudinal case of a left middle cerebral artery aneurysm, which demonstrated growth at 7 months and subsequent enlargement with rupture at 11 months. The location of de novo bleb formation corresponded to the initial high WSS region (20.3 Pa), suggesting that aneurysm growth may also occur in high WSS environ-

ments. In 2023, Tsuji *et al.* [19] conducted an observational study of 215 unruptured small aneurysms and found that the HSCR was significantly higher in 33 growing aneurysms compared with stable ones and was identified as a key predictor of growth in small IAs. Elevated HSCR indicates that high WSS is concentrated in a limited area, and IA growth is promoted via the induction of localized vascular wall injury.

Nevertheless, these studies largely treated IA growth as a single global phenomenon without distinguishing distinct growth patterns. In fact, studies have demonstrated that different hemodynamic environments lead to distinct IA growth patterns. In 2017, Machi *et al.* [29] classified six aneurysms into two growth patterns: a "focal growth group" (localized bleb formation at the dome) and a "global growth group" (overall aneurysm enlargement with neck widening). Focal growth was predominantly observed in dome regions characterized by low WSS and high OSI, whereas global growth was more frequently associated with regions of high WSS and high WSSG.

In 2025, Fukuda *et al.* [15] further investigated the relationship between hemodynamics and growth patterns by stratifying aneurysms into two size groups (<4 mm and ≥4 mm). It was demonstrated that small aneurysms presented higher TAWSS and TAWSSG, as well as elevated transWSS at the aneurysm neck and parent artery, and predominantly exhibited a global growth pattern. By comparison, larger aneurysms had higher NtransWSS at the aneurysm dome and were more prone to focal dome growth.

In the same year, Karnam *et al.* [30] further analyzed aneurysm growth patterns based on location, wall segmentation, and flow direction. It was reported that growth in anterior communicating artery aneurysms and sidewall aneurysms predominantly occurred in the aneurysm body and was associated with high-flow impingement, where elevated WSS contributed to wall degeneration and thinning. In contrast, middle cerebral artery aneurysms and bifurcation aneurysms more commonly exhibited growth at both the dome and body, which was attributed to slow and oscillatory flow in the dome and central regions, leading to wall thickening and remodeling. From the perspective of flow-directional segmentation, growth was most frequently concentrated in the central region across all aneurysm types. Anterior communicating artery aneurysms demonstrated growth tendencies in both inflow and central regions, whereas middle cerebral artery aneurysms were more likely to grow in the central region alone.

Overall, these findings suggest that IA growth is not driven by a single hemodynamic mechanism but is instead influenced by a combination of aneurysm size, anatomical location, morphological characteristics, and local hemodynamic environment.

5. Research Progress on CFD-Based Assessment of Intracranial Aneurysm Rupture

Most CFD studies investigating IA rupture have employed cross-sectional de-

signs, comparing ruptured and unruptured aneurysms from different patients. Although these studies have identified important hemodynamic features associated with rupture, causal interpretation is limited due to potential confounding from inter-patient variability, including demographic characteristics, vascular risk factors, and genetic background. Moreover, post-rupture morphological changes, such as alterations in aneurysm geometry and thrombus formation, may affect CFD-derived parameters and prevent accurate representation of the pre-rupture hemodynamic state.

To overcome these limitations, longitudinal studies have been performed to evaluate hemodynamic changes within the same aneurysm before and after rupture, providing stronger evidence regarding temporal associations and reducing inter-patient variability [11] [33]. In addition, mirror aneurysm studies, which utilize bilateral aneurysms within the same patient as a self-controlled model, have gained increasing attention for minimizing patient-related confounding factors [34] [35]. CFD parameters for IA rupture assessment are categorized into quantitative and qualitative types, and the following review is organized accordingly.

5.1. Advances in Quantitative Parameters in IA Rupture

IA rupture has been associated with multiple quantitative hemodynamic parameters, with current research focusing primarily on WSS, OSI, RRT, and LSA. A summary of the parameters used and the main findings across studies is provided in Table 3.

Table 3. Summary of studies investigating the relationship between aneurysmal hemodynamics and rupture risk.

Author	Year	Number and grouping of aneurysms	Hemodynamic parameters	CFD method	Main findings
Bozorgpour [12]	2025	6 cases (ruptured/unruptured: 3/3)	WSS, TAWSS, OSI, RRT, ECAP	Pulsatile inflow waveform; Newtonian fluid; rigid vessel wall	Ruptured IAs were characterized by decreased WSS and TAWSS, and increased OSI, RRT, and ECAP; regions of elevated OSI and RRT frequently co-localized with vortex cores.
Hejčl *et al.* [10]	2023	6 cases (all ruptured)	TAWSS, OSI, LSA, PWSS, etc.	Time-dependent inflow waveform; Newtonian fluid; rigid vessel wall	Four rupture sites were located in regions of low WSS and high OSI, typically accompanied by vortex formation; one occurred in a high-WSS jet impingement region, and one within a bleb region characterized by low WSS and low OSI.
Fujimura *et al.* [11]	2023	21 cases (same aneurysms before and after rupture)	NWSS (mean/max/min), NWSSD, PD, OSI, LSA, LSI, SCI, VFR, ICI, etc.	Standardized pulsatile inflow waveform; Newtonian fluid; rigid vessel wall	In most IAs, NWSS decreased after rupture; in a minority of cases, NWSS increased due to post-SAH vasospasm and consequent inflow narrowing.

Continued

Zhu *et al.* [33]	2023	3 cases (ruptured/unruptured: 2/1)	NWSS, OSI, RRT	Standardized pulsatile inflow waveform; Newtonian fluid; rigid vessel wall	OSI increased following IA rupture; both high and low NWSS may contribute to rupture at different stages.
Xu *et al.* [36]	2022	49 cases (ruptured/unruptured: 23/26)	NWSS, OSI, LSAR, NP, RRT	Standardized pulsatile inflow waveform; Newtonian fluid; rigid vessel wall	The ruptured group exhibited lower NWSS and higher OSI; NWSS was identified as an independent hemodynamic risk factor for rupture of A1 segment aneurysms.
Yuan *et al.* [35]	2021	144 cases (72 mirror pairs, each with one ruptured and one unruptured aneurysm)	NWSS, WSS mean, LSA%, OSI, RRT, etc.	Patient-specific pulsatile inflow waveforms from transcranial Doppler; Newtonian fluid; rigid vessel wall	The ruptured group demonstrated higher LSA% and lower NWSS and mean WSS; all three parameters were independent risk factors for IA rupture.
Perera *et al.* [37]	2020	48 cases (ruptured/unruptured: 10/38)	OSI, RRT, TAWSS, ICI	Standardized pulsatile inflow waveform; Newtonian fluid; rigid vessel wall	OSImax, OSImean, RRTmean, and RRTmax were elevated in the ruptured group, with; OSImean identified as an independent predictor.
Neyazi *et al.* [38]	2020	87 cases (ruptured/unruptured: 38/49)	RRT (max/mean), OSI (max/mean), LSA, ICI, SCI, etc.	Standardized flow waveforms from healthy volunteers; Newtonian fluid; rigid vessel wall	The combination of aspect ratio (AR) and RRTmax provided improved performance in rupture risk assessment.
Detmer *et al.* [39]	2019	1931 cases (ruptured/unruptured: 558/1373)	WSS (max/min/mean), LSA, SCI, ICI, etc.	Flow conditions based on PC-MRI data from healthy subjects; Newtonian fluid; rigid vessel wall	Ruptured IAs were associated with higher WSS and OSI, as well as more complex and unstable flow patterns.
Liu *et al.* [40]	2019	192 cases (ruptured/unruptured: 96/96)	NWSS (mean/max), OSI, RRT, LSAR, WSSG, etc.	Pulsatile inflow waveform; Newtonian fluid; rigid vessel wall	Intraoperatively ruptured IAs exhibited lower NWSSmax and higher OSI; both were independent risk factors.
Zhang *et al.* [41]	2016	206 cases (ruptured/unruptured: 73/133)	TAWSS, WSS (max/min), OSI, LSA	Pulsatile inflow waveform; Newtonian fluid; rigid vessel wall	The ruptured group showed larger LSA and lower TAWSS, WSSmax and WSSmin compared with the unruptured group; LSA was an independent predictor of rupture in VSIAs.
Cebral *et al.* [13]	2011	210 cases (rupture status not explicitly stratified)	ICI, MWSS, SCI, VDR, LSA, LSI, KER	Pulsatile inflow waveform; Newtonian fluid; rigid vessel wall	Ruptured IAs demonstrated increased ICI, MWSS, and SCI, and decreased VDR.

The results of existing studies indicate that inconsistent conclusions have been reported regarding the relationship between WSS and IA rupture, leading to the proposal of two competing hypotheses: the "high-WSS theory" and the "low-WSS theory." Although these hypotheses appear contradictory, they in fact reflect the complex mechanisms of IA rupture under distinct hemodynamic environments. From a pathophysiological perspective, Meng *et al.* [31] proposed that elevated WSS may promote the release of matrix metalloproteinases and induce smooth muscle cell apoptosis, whereas low WSS accompanied by high OSI may trigger inflammation-mediated destructive vascular remodeling. Both pathways may ultimately weaken aneurysm wall integrity and contribute to rupture.

As a parameter closely related to WSS, OSI reflects the temporal fluctuation of flow direction, with higher values indicating reduced flow stability and typically exhibiting a negative correlation with WSS. Existing studies [12] [33] [36] [37] [39] [40] have consistently demonstrated that elevated OSI is associated with IA rupture.

RRT quantifies the residence time of blood within the aneurysm sac, with higher values indicating prolonged blood stagnation. Previous studies [12] [37] [38] have reported that ruptured IAs are commonly characterized by increased RRT, suggesting exposure of the aneurysm wall to a stagnant and unstable flow environment. However, such abnormal hemodynamic values are often derived from specific intra-aneurysmal flow patterns; therefore, integration with qualitative flow characteristics is required to further elucidate rupture-related hemodynamic mechanisms.

5.2. Advances in Qualitative Parameters in IA Rupture

In addition to quantitative parameters, qualitative indicators such as flow patterns also serve as crucial factors affecting IA rupture. Differences in local hemodynamic features, including vortical structures and flow impingement, may trigger diverse biological effects, thereby facilitating the weakening, degeneration, and remodeling of the aneurysm wall [42].

In existing CFD-based studies, qualitative flow analysis has been more frequently applied to evaluate post-treatment hemodynamic remodeling following surgical or endovascular interventions, whereas relatively fewer studies have used qualitative parameters as primary variables to directly compare ruptured and unruptured IAs. In 2011, Cebral *et al.* [43] analyzed 210 aneurysms and reported that ruptured IAs were characterized by complex and unstable flow patterns, as well as concentrated inflow jets. Subsequent studies further confirmed that ruptured aneurysms are more frequently associated with multi-vortex and chaotic flow structures, accompanied by stronger and more concentrated inflow jets [10] [44] [45]. In 2021, Xu *et al.* [46] demonstrated that both complex flow patterns and the size of the impingement region were independent risk factors for rupture in internal carotid artery aneurysms. More recently, in 2025, Vu *et al.* [47] classified IA flow patterns and reported that rupture status was significantly associated with higher

proportions of Type 3 (flow direction changes with a single vortex) and Type 4 (dynamic formation and dissipation of multiple vortices with changing flow direction) complex flow patterns compared with unruptured aneurysms.

In summary, the hemodynamic characteristics associated with IA rupture are highly complex, and no single parameter is sufficient to fully characterize rupture risk. An integrated approach combining both qualitative and quantitative CFD-derived parameters is therefore required for a more comprehensive and accurate evaluation of IA rupture risk from a multidimensional perspective.

6. Conclusion

CFD technology has provided important insights into the hemodynamic mechanisms underlying intracranial aneurysm formation, progression, and rupture by enabling comprehensive evaluation of complex blood flow characteristics, including quantitative hemodynamic parameters and qualitative flow patterns. Although CFD-derived parameters have demonstrated potential for aneurysm risk stratification, their clinical application requires further validation in longitudinal cohorts to determine whether baseline hemodynamic characteristics can predict subsequent aneurysm growth or rupture. Moreover, the incremental predictive value of CFD parameters beyond established clinical and morphological predictors should be systematically evaluated to determine their added contribution to individualized risk assessment. Future studies integrating CFD with advanced imaging modalities, artificial intelligence, and longitudinal clinical data may facilitate the development of more accurate predictive models and promote the translation of CFD-based approaches into personalized aneurysm management.

Conflicts of Interest

The authors declare no conflicts of interest regarding the publication of this paper.

References

[1] Claassen, J. and Park, S. (2022) Spontaneous Subarachnoid Haemorrhage. *The Lancet*, **400**, 846-862. https://doi.org/10.1016/s0140-6736(22)00938-2

[2] Korja, M. and Kaprio, J. (2016) Controversies in Epidemiology of Intracranial Aneurysms and Sah. *Nature Reviews Neurology*, **12**, 50-55. https://doi.org/10.1038/nrneurol.2015.228

[3] Long, H., Che, W., Yang, C., Liao, Y., Wu, J., Chen, C., *et al.* (2025) Identification of Key Risk Factors for Rupture in Small Intracranial Aneurysms: A Multicenter Study. *World Neurosurgery*, **194**, Article ID: 123552. https://doi.org/10.1016/j.wneu.2024.12.011

[4] Paritala, P.K., Anbananthan, H., Hautaniemi, J., Smith, M., George, A., Allenby, M., *et al.* (2023) Reproducibility of the Computational Fluid Dynamic Analysis of a Cerebral Aneurysm Monitored over a Decade. *Scientific Reports*, **13**, Article No. 219. https://doi.org/10.1038/s41598-022-27354-w

[5] Chitwood, C.A., Shih, E.D., Amili, O., Larson, A.S., Ogle, B.M., Alford, P.W., *et al.* (2022) Biology and Hemodynamics of Aneurysm Rupture. *Neurosurgery Clinics of*

North America, **33**, 431-441. https://doi.org/10.1016/j.nec.2022.06.002

[6] Karmonik, C., Diaz, O., Klucznik, R., Grossman, R.G., Zhang, Y.J., Britz, G., *et al.* (2015) Quantitative Comparison of Hemodynamic Parameters from Steady and Transient CFD Simulations in Cerebral Aneurysms with Focus on the Aneurysm Ostium. *Journal of NeuroInterventional Surgery*, **7**, 367-372. https://doi.org/10.1136/neurintsurg-2014-011182

[7] Diab, R., Chang, D., Zhu, C., Levitt, M.R., Aksakal, M., Zhao, H., *et al.* (2023) Advanced Cross-Sectional Imaging of Cerebral Aneurysms. *The British Journal of Radiology*, **96**, Article ID: 20220686. https://doi.org/10.1259/bjr.20220686

[8] Youn, S.W. and Lee, J. (2022) From 2D to 4D Phase-Contrast MRI in the Neurovascular System: Will It Be a Quantum Jump or a Fancy Decoration? *Journal of Magnetic Resonance Imaging*, **55**, 347-372. https://doi.org/10.1002/jmri.27430

[9] Yi, H., Yang, Z., Bramlage, L. and Ludwig, B. (2024) Using DFT on Ultrasound Measurements to Determine Patient-Specific Blood Flow Boundary Conditions for Computational Hemodynamics of Intracranial Aneurysms. *Computers in Biology and Medicine*, **176**, Article ID: 108563. https://doi.org/10.1016/j.compbiomed.2024.108563

[10] Hejčl, A., Brunátová, J., Švihlová, H., Víteček, J., Wünschová, A.V., Sejkorová, A., *et al.* (2024) Rupture Point Is Associated with Divergent Hemodynamics in Intracranial Aneurysms. *Frontiers in Neurology*, **15**, Article 1364105. https://doi.org/10.3389/fneur.2024.1364105

[11] Fujimura, S., Yamanaka, Y., Takao, H., Ishibashi, T., Otani, K., Karagiozov, K., *et al.* (2023) Hemodynamic and Morphological Differences in Cerebral Aneurysms between before and after Rupture. *Journal of Neurosurgery*, **140**, 774-782. https://doi.org/10.3171/2023.6.jns23289

[12] Bozorgpour, R. (2026) Hemodynamic Markers: CFD-Based Prediction of Cerebral Aneurysm Rupture Risk. *Vascular Pharmacology*, **162**, Article ID: 107578. https://doi.org/10.1016/j.vph.2025.107578

[13] Cebral, J.R., Mut, F., Weir, J. and Putman, C. (2011) Quantitative Characterization of the Hemodynamic Environment in Ruptured and Unruptured Brain Aneurysms. *American Journal of Neuroradiology*, **32**, 145-151. https://doi.org/10.3174/ajnr.a2419

[14] Peiffer, V., Sherwin, S.J. and Weinberg, P.D. (2013) Computation in the Rabbit Aorta of a New Metric—The Transverse Wall Shear Stress—To Quantify the Multidirectional Character of Disturbed Blood Flow. *Journal of Biomechanics*, **46**, 2651-2658. https://doi.org/10.1016/j.jbiomech.2013.08.003

[15] Fukuda, S., Shimogonya, Y., Watanabe, A., Yonemoto, N., Fukuda, M. and Yasoda, A. (2025) Two Possible Hemodynamic Mechanisms Underlying the Growth of Cerebral Aneurysms Depending on Their Size: The NHO CFD ABO Study. *Journal of Cerebral Blood Flow & Metabolism*, **45**, 1581-1592. https://doi.org/10.1177/0271678x251325972

[16] Xiang, J., Natarajan, S.K., Tremmel, M., Ma, D., Mocco, J., Hopkins, L.N., *et al.* (2011) Hemodynamic-Morphologic Discriminants for Intracranial Aneurysm Rupture. *Stroke*, **42**, 144-152. https://doi.org/10.1161/strokeaha.110.592923

[17] Shimogonya, Y., Ishikawa, T., Imai, Y., Matsuki, N. and Yamaguchi, T. (2009) Can Temporal Fluctuation in Spatial Wall Shear Stress Gradient Initiate a Cerebral Aneurysm? A Proposed Novel Hemodynamic Index, the Gradient Oscillatory Number (GON). *Journal of Biomechanics*, **42**, 550-554. https://doi.org/10.1016/j.jbiomech.2008.10.006

[18] Weiss, A.J., Panduro, A.O., Schwarz, E.L., Sexton, Z.A., Lan, I.S., Geisbush, T.R., *et al.* (2023) A Matched-Pair Case Control Study Identifying Hemodynamic Predictors of Cerebral Aneurysm Growth Using Computational Fluid Dynamics. *Frontiers in Physiology*, **14**, Article 1300754. https://doi.org/10.3389/fphys.2023.1300754

[19] Tsuji, M., Ishida, F., Yasuda, R., Sato, T., Furukawa, K., Miura, Y., *et al.* (2024) Computational Fluid Dynamics for Predicting the Growth of Small Unruptured Cerebral Aneurysms. *Journal of Neurosurgery*, **140**, 138-143. https://doi.org/10.3171/2023.5.jns222752

[20] Suzuki, T., Takao, H., Suzuki, T., Kambayashi, Y., Watanabe, M., Sakamoto, H., *et al.* (2016) Determining the Presence of Thin-Walled Regions at High-Pressure Areas in Unruptured Cerebral Aneurysms by Using Computational Fluid Dynamics. *Neurosurgery*, **79**, 589-595. https://doi.org/10.1227/neu.0000000000001232

[21] Nakatani, H., Hashimoto, N., Kang, Y., Yamazoe, N., Kikuchi, H., Yamaguchi, S., *et al.* (1991) Cerebral Blood Flow Patterns at Major Vessel Bifurcations and Aneurysms in Rats. *Journal of Neurosurgery*, **74**, 258-262. https://doi.org/10.3171/jns.1991.74.2.0258

[22] Meng, H., Wang, Z., Hoi, Y., Gao, L., Metaxa, E., Swartz, D.D., *et al.* (2007) Complex Hemodynamics at the Apex of an Arterial Bifurcation Induces Vascular Remodeling Resembling Cerebral Aneurysm Initiation. *Stroke*, **38**, 1924-1931. https://doi.org/10.1161/strokeaha.106.481234

[23] Can, A. and Du, R. (2016) Association of Hemodynamic Factors with Intracranial Aneurysm Formation and Rupture: Systematic Review and Meta-Analysis. *Neurosurgery*, **78**, 510-520. https://doi.org/10.1227/neu.0000000000001083

[24] Zhai, X., Wang, Y., Fang, G., Hu, P., Zhang, H. and Zhu, C. (2022) Case Report: Dynamic Changes in Hemodynamics during the Formation and Progression of Intracranial Aneurysms. *Frontiers in Cardiovascular Medicine*, **8**, Article 775536. https://doi.org/10.3389/fcvm.2021.775536

[25] Yang, H., Kim, J.J., Kim, Y.B., Cho, K.C. and Oh, J.H. (2024) Investigation of Paraclinoid Aneurysm Formation by Comparing the Combined Influence of Hemodynamic Parameters between Aneurysmal and Non-Aneurysmal Arteries. *Journal of Cerebral Blood Flow & Metabolism*, **44**, 1393-1403. https://doi.org/10.1177/0271678x231218589

[26] Nishiwaki, T., Ikedo, T., Kushi, Y., Shimonaga, K., Kobayashi, H., Itazu, T., *et al.* (2024) Hemodynamic Differences Determining Rupture and Non-Rupture in Middle Cerebral Aneurysms after Growth. *PLOS ONE*, **19**, e0307495. https://doi.org/10.1371/journal.pone.0307495

[27] Brinjikji, W., Chung, B.J., Jimenez, C., Putman, C., Kallmes, D.F. and Cebral, J.R. (2016) Hemodynamic Differences between Unstable and Stable Unruptured Aneurysms Independent of Size and Location: A Pilot Study. *Journal of NeuroInterventional Surgery*, **9**, 376-380. https://doi.org/10.1136/neurintsurg-2016-012327

[28] Cornelissen, B.M.W., Leemans, E.L., Slump, C.H., van den Berg, R., Marquering, H.A. and Majoie, C.B.L.M. (2022) Hemodynamic Changes after Intracranial Aneurysm Growth. *Journal of Neurosurgery*, **136**, 1738-1744. https://doi.org/10.3171/2021.6.jns204155

[29] Machi, P., Ouared, R., Brina, O., Bouillot, P., Yilmaz, H., Vargas, M.I., *et al.* (2019) Hemodynamics of Focal versus Global Growth of Small Cerebral Aneurysms. *Clinical Neuroradiology*, **29**, 285-293. https://doi.org/10.1007/s00062-017-0640-6

[30] Karnam, Y., Mut, F., Robertson, A.M., Kaneko, N. and Cebral, J.R. (2025) Competing Pathways of Intracranial Aneurysm Growth: Linking Regional Growth Distribution

and Hemodynamics. *Journal of Neurosurgery*, **142**, 1741-1750. https://doi.org/10.3171/2024.9.jns241208

[31] Meng, H., Tutino, V.M., Xiang, J. and Siddiqui, A. (2014) High WSS or Low WSS? Complex Interactions of Hemodynamics with Intracranial Aneurysm Initiation, Growth, and Rupture: Toward a Unifying Hypothesis. *American Journal of Neuroradiology*, **35**, 1254-1262. https://doi.org/10.3174/ajnr.a3558

[32] Wang, Y., Leng, X., Zhou, X., Li, W., Siddiqui, A.H. and Xiang, J. (2018) Hemodynamics in a Middle Cerebral Artery Aneurysm before Its Growth and Fatal Rupture: Case Study and Review of the Literature. *World Neurosurgery*, **119**, e395-e402. https://doi.org/10.1016/j.wneu.2018.07.174

[33] Zhu, Y., Zou, R., Sun, X., Lei, X., Xiang, J., Guo, Z., *et al.* (2023) Assessing the Risk of Intracranial Aneurysm Rupture Using Computational Fluid Dynamics: A Pilot Study. *Frontiers in Neurology*, **14**, Article 1277278. https://doi.org/10.3389/fneur.2023.1277278

[34] Yong-Wei, H., Wang, X.Y., Li, Z.P. and Yin, X.S. (2023) The Rupture Risk Factors of Mirror Intracranial Aneurysms: A Systematic Review and Meta-Analysis Based on Morphological and Hemodynamic Parameters. *PLOS ONE*, **18**, e0286249. https://doi.org/10.1371/journal.pone.0286249

[35] Yuan, J., Huang, C., Li, Z., Jiang, X., Zhao, X., Wu, D., *et al.* (2021) Hemodynamic and Morphological Parameters of Ruptured Mirror Posterior Communicating Artery Aneurysms. *Frontiers in Neurology*, **12**, Article 653589. https://doi.org/10.3389/fneur.2021.653589

[36] Xu, M., Lv, N., Sun, K., Hong, R., Wang, H., Wang, X., *et al.* (2022) Morphological and Hemodynamic Risk Factors for the Rupture of Proximal Anterior Cerebral Artery Aneurysms (A1 Segment). *Frontiers in Aging Neuroscience*, **14**, Article 835373. https://doi.org/10.3389/fnagi.2022.835373

[37] Perera, R., Isoda, H., Ishiguro, K., Mizuno, T., Takehara, Y., Terada, M., *et al.* (2020) Assessing the Risk of Intracranial Aneurysm Rupture Using Morphological and Hemodynamic Biomarkers Evaluated from Magnetic Resonance Fluid Dynamics and Computational Fluid Dynamics. *Magnetic Resonance in Medical Sciences*, **19**, 333-344. https://doi.org/10.2463/mrms.mp.2019-0107

[38] Neyazi, B., Swiatek, V.M., Skalej, M., Beuing, O., Stein, K., Hattingen, J., *et al.* (2020) Rupture Risk Assessment for Multiple Intracranial Aneurysms: Why There Is No Need for Dozens of Clinical, Morphological and Hemodynamic Parameters. *Therapeutic Advances in Neurological Disorders*, **13**. https://doi.org/10.1177/1756286420966159

[39] Detmer, F.J., Chung, B.J., Jimenez, C., Hamzei-Sichani, F., Kallmes, D., Putman, C., *et al.* (2019) Associations of Hemodynamics, Morphology, and Patient Characteristics with Aneurysm Rupture Stratified by Aneurysm Location. *Neuroradiology*, **61**, 275-284. https://doi.org/10.1007/s00234-018-2135-9

[40] Liu, Q., Jiang, P., Wu, J., Gao, B. and Wang, S. (2019) The Morphological and Hemodynamic Characteristics of the Intraoperative Ruptured Aneurysm. *Frontiers in Neuroscience*, **13**, Article 233. https://doi.org/10.3389/fnins.2019.00233

[41] Zhang, Y., Tian, Z., Jing, L., Zhang, Y., Liu, J. and Yang, X. (2016) Bifurcation Type and Larger Low Shear Area Are Associated with Rupture Status of Very Small Intracranial Aneurysms. *Frontiers in Neurology*, **7**, Article 169. https://doi.org/10.3389/fneur.2016.00169

[42] Karnam, Y., Mut, F., Yu, A.K., Cheng, B., Amin-Hanjani, S., Charbel, F.T., *et al.* (2024) Description of the Local Hemodynamic Environment in Intracranial Aneu-

rysm Wall Subdivisions. *International Journal for Numerical Methods in Biomedical Engineering*, **40**, e3844. https://doi.org/10.1002/cnm.3844

[43] Cebral, J.R., Mut, F., Weir, J. and Putman, C.M. (2011) Association of Hemodynamic Characteristics and Cerebral Aneurysm Rupture. *American Journal of Neuroradiology*, **32**, 264-270. https://doi.org/10.3174/ajnr.a2274

[44] Salimi Ashkezari, S.F., Mut, F., Slawski, M., Jimenez, C.M., Robertson, A.M. and Cebral, J.R. (2022) Identification of Small, Regularly Shaped Cerebral Aneurysms Prone to Rupture. *American Journal of Neuroradiology*, **43**, 547-553. https://doi.org/10.3174/ajnr.a7470

[45] Doddasomayajula, R., Chung, B., Hamzei-Sichani, F., Putman, C.M. and Cebral, J.R. (2017) Differences in Hemodynamics and Rupture Rate of Aneurysms at the Bifurcation of the Basilar and Internal Carotid Arteries. *American Journal of Neuroradiology*, **38**, 570-576. https://doi.org/10.3174/ajnr.a5088

[46] Xu, W.D., Shi, Z., Hu, B., Zhang, L.J. and Lu, G.M. (2021) Hemodynamics-Based Analysis of Factors Associated with Aneurysm Rupture in Different Sides of the Internal Carotid Artery. *Chinese Journal of Medical History*, **101**, 1798-1804. (In Chinese) https://doi.org/10.3760/cma.j.cn112137-20210119-00168

[47] Vu, D.L., Nguyen, V.H., Nguyen, H.A., Nguyen, Q.A., Tran, A.T., Le, H.K., *et al.* (2025) Hemodynamic Characteristics in Ruptured and Unruptured Intracranial Aneurysms: A Prospective Cohort Study Utilizing the Aneurysmflow Tool. *American Journal of Neuroradiology*, **46**, 75-83. https://doi.org/10.3174/ajnr.a8444